Wavelength-Dependent Photolysis of *n*-Butyraldehyde and *i*-Butyraldehyde in the 280−330-nm Region

Yunqing Chen and Lei Zhu*

Wadsworth Center, New York State Department of Health, Department of Environmental Health and Toxicology, State University of New York, Albany, New York 12201-0509

Joseph S. Francisco

Department of Chemistry, Purdue University, West Lafayette, Indiana 47907

Received: December 18, 2001; In Final Form: June 17, 2002

We have investigated the gas-phase photolysis of *n*-butyraldehyde ($CH_3(CH_2)_2CHO$) and *i*-butyraldehyde ($(CH_3)_2CHCHO$) at 5 nm intervals in the 280−330 nm region using dye laser photolysis in combination with cavity ring-down spectroscopy. Absorption cross sections of both aldehydes have been measured. The quantum yields of radical/molecular photolysis products have been determined as functions of photodissociation wavelength (λ), aldehyde pressure, and nitrogen buffer-gas pressure. The HCO radical is a photodecomposition product of both aldehydes. The HCO quantum yields, determined by monitoring HCO absorption at 613.8 nm, decrease with increasing aldehyde pressure in the 1−10 Torr range because of the increasing HCO + HCO, HCO + R, and HCO + RCHO reactions (R = *n*-C_3H_7 and *i*-C_3H_7) at higher aldehyde pressures and because of quenching by ground-state aldehydes. After separation of the contribution of HCO radical reactions, the aldehyde pressure quenching effect was observed only at $\lambda \geq 310$ nm. The HCO quantum yields (at all λ values) and the ratios of quenching to unimolecular decay rate constants of excited aldehydes ($\lambda \geq 310$ nm) are given. The HCO quantum yields from *n*-butyraldehyde photolysis are 0.52 ± 0.05, 0.74 ± 0.08, 0.84 ± 0.04, and 0.77 ± 0.08 at 305, 310, 315, and 320 nm, respectively, where the uncertainty (1σ) represents experimental scatter only. The corresponding HCO quantum yields from *i*-butyraldehyde photolysis are 0.92 ± 0.08, 1.06 ± 0.07, 1.06 ± 0.13, and 1.10 ± 0.10. The differences in the peak HCO quantum yields are attributed to the opening up of the Norrish II channel (formation of $C_2H_4 + CH_3CHO$) from *n*-butyraldehyde photolysis. The dependence of the HCO quantum yield on the nitrogen buffer-gas pressure was examined between 8 and 400 Torr; no dependence was observed. The end products from the photolysis of both aldehydes were analyzed by mass spectrometry. The occurrence of the Norrish II channel is confirmed for *n*-butyraldehyde.

Introduction

Aliphatic aldehydes are key trace components of the troposphere. They play a central role in the formation of photochemical smog, peroxyacetyl nitrate (PAN), and ground-level ozone. Photodissociation of aldehydes is an important source of free radicals in the atmosphere. The major gas-phase removal pathways for saturated aldehydes in the atmosphere are unimolecular photodissociation and reactions with OH radicals. Previous studies have reported rate constants for reactions of OH radicals with C_1-C_5 aldehydes.[1−5] Extensive investigations have been carried out to determine the photolysis of formaldehyde (CH_2O) and acetaldehyde (CH_3CHO).[6−9] Recently, our group has studied the wavelength-dependent photolysis of propionaldehyde (C_2H_5CHO), *n*-pentanal (*n*-C_4H_9CHO), *i*-pentanal (*i*-C_4H_9CHO), and *t*-pentanal (*t*-C_4H_9CHO).[10−12] In the case of *n*-pentanal photolysis, the Norrish II channel (formation of $CH_3CHO + C_3H_6$) occurs at the expense of the radical-formation channel. The yields of the Norrish II and radical-formation channels are comparable for *i*-pentanal. The Norrish II channel is not available for *t*-pentanal. Because *n*-butyraldehyde (*n*-C_3H_7CHO; *n*-butanal) is the smallest aliphatic aldehyde capable of the Norrish II process (formation of $CH_3CHO + C_2H_4$), it would be interesting to compare its photolysis with that of *n*-pentanal and *i*-pentanal. The photolysis of *n*-butyraldehyde has been reported at 313 nm.[13] There has been a recent study of the broadband oxidation of *n*-butyraldehyde in air over the 275−380 nm region.[14] Photooxidation of *i*-butyraldehyde (*i*-C_3H_7CHO; *i*-butanal) has been investigated at 253.7, 280.3, 302.2, 312.8, 326.1, and 334.1 nm.[15] Determination of the wavelength-dependent photolysis yields of C_4 aldehydes allows us to make a comparison with the yields obtained previously for C_1-C_3 and C_5 aldehydes. Comparison of the HCO yields from the photodecomposition of *n*-butyraldehyde and *i*-butyraldehyde also allows us to determine the effect of alkyl substitution on aldehyde photolysis quantum yields.

n-Butyraldehyde and *i*-butyraldehyde possess a UV absorption band in the 240−360 nm region resulting from an $n \rightarrow \pi^*$ transition.[16] The following dissociation pathways are energetically possible following excitation of *n*-butyraldehyde and *i*-butyraldehyde in the UV region:

* To whom correspondence should be addressed. E-mail: zhul@orkney.ph.albany.edu. Fax: (518) 473-2895.

10.1021/jp014544e CCC: $22.00
Published on Web 07/26/2002

$$RCHO + h\nu \rightarrow R + HCO \ (\lambda \leq 349 \text{ nm for } R = n\text{-}C_3H_7 \text{ and } i\text{-}C_3H_7) \quad (1)$$

$$\rightarrow RH + CO \ (\text{all } \lambda) \quad (2)$$

$$\rightarrow CH_3CHO + C_2H_4 \ (\lambda \leq 1.3\ \mu\text{m for } R = n\text{-}C_3H_7) \quad (3)$$

$$\rightarrow RCO + H \ (\lambda \leq 327 \text{ nm for } R = n\text{-}C_3H_7 \text{ and } i\text{-}C_3H_7) \quad (4)$$

Threshold wavelengths were calculated from the corresponding enthalpy changes. Pathways 1, 2, and 3 are radical-formation, molecular-elimination, and Norrish II processes, respectively. Pathway 4 is another radical-formation channel but is found to be minor for small aldehydes.[17]

Presented in this paper are the results obtained from an experimental investigation of the photolysis of *n*-butyraldehyde and *i*-butyraldehyde at 5-nm intervals in the 280−330 nm region using dye laser photolysis combined with cavity ring-down spectroscopy.[18,19] Absorption cross sections of *n*-butyraldehyde and *i*-butyraldehyde have been obtained at each wavelength that was studied. The quantum yields of HCO and their dependences on photolysis wavelength, aldehyde pressure, and total pressure have been determined. Absolute HCO radical concentrations were calibrated relative to those obtained from formaldehyde photolysis or from the $Cl + H_2CO \rightarrow HCl + HCO$ reaction. The photolysis end-products have been characterized by mass spectrometry at 290, 310, and 330 nm. Photodissociation rate constants and lifetimes of *n*-butyraldehyde and *i*-butyraldehyde have been estimated as a function of zenith angle for cloudless conditions at sea level and at 760 Torr of nitrogen.

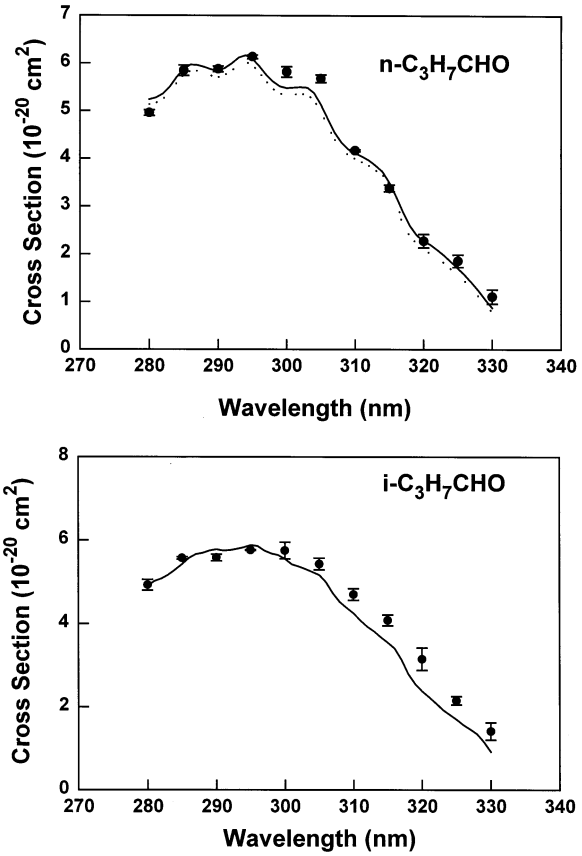

Figure 1. Absorption cross sections of *n*-butyraldehyde (upper panel) and *i*-butyraldehyde (lower panel) in the 280−330-nm region: (●) this work; (—) Martinez and co-workers;[16] (· · ·) Tadic and co-workers.[14]

Experimental Technique

The experimental apparatus has been described in detail elsewhere.[11,12,20,21] Two laser systems, one for the photolysis of aldehydes and the other for the detection of the HCO photoproduct, were used in the experiments. Photolysis radiation was provided by the frequency-doubled output of a tunable dye laser pumped by a 308-nm XeCl excimer laser (~200 mJ/pulse). Laser dyes used in the experiments included coumarin 153, rhodamine 6G, rhodamine B, rhodamine 101, and DCM. The photolysis beam was introduced into the reaction cell at a 15° angle with respect to the main cell axis through a sidearm. The probe laser pulse (613−617 nm) from a dye laser pumped by a nitrogen laser was directed along the main optical axis of the cell. The pump and the probe laser beams crossed one another at the center of the reaction cell, which was vacuum-sealed with a pair of high-reflectance cavity mirrors. The base path length between the two cavity mirrors was 50 cm. A fraction of the probe laser pulse was injected into the cavity through the front mirror. The light-intensity decay inside the cavity was measured by monitoring the weak transmission of light through the rear mirror with a photomultiplier tube (PMT). The PMT output was amplified, digitized, and sent to a computer. The decay curve was fitted to a single-exponential decay function. The ring-down time constant and the total loss per optical pass were computed. The ring-down time constant was on the order of 27 μs for an empty cavity, with 60 ppm transmission loss per mirror. In the presence of absorbing species, the cavity decay time shortened. By measurement of the cavity losses with and without a photolysis pulse, the HCO absorption from the photolysis of *n*-butyraldehyde or *i*-butyraldehyde was obtained. A pulse/delay generator was used to vary the delay time between the firing of the photodissociation and the probe lasers. The photolysis laser pulse energy was measured with a calibrated joulemeter. The mass spectra of the stable end-products from photodecomposition of *n*-butyraldehyde and *i*-butyraldehyde were recorded by a residual gas analyzer mass spectrometer (Stanford Research Systems, RGA300), which was connected on-line with the photolysis cell.

Gas pressure was measured at the center of the reaction cell with a Baratron capacitance manometer. Quantum yield measurements were made at a laser repetition rate of 0.1 Hz to ensure replenishment of gas samples between successive laser pulses. The spectrum scan was performed at a laser repetition rate of 1 Hz. All experiments were carried out at an ambient temperature of 293 ± 2 K.

n-Butyraldehyde and *i*-butyraldehyde (both with purity ≥99.5%; Aldrich) were purified by repeated vacuum distillations at 77 K before each experimental run to remove volatile impurities. Formaldehyde was generated by pyrolysis of polymer paraformaldehyde (≥95% purity; Aldrich) at 110 °C. Nitrogen (≥99.999% purity; Northeast Gas Technology) and chlorine (≥99.5% purity; Matheson) were used without further purification.

Results and Discussion

Absorption Cross Sections of *n*-Butyraldehyde and *i*-Butyraldehyde in the 280−330-nm Region. Shown in Figure 1 and Table 1 are the room-temperature absorption cross sections of *n*-butyraldehyde and *i*-butyraldehyde determined at 5-nm intervals in the 280−330-nm region. The absorption cross section at each wavelength was obtained by monitoring the transmitted photolysis photon intensity as a function of *n*-

TABLE 1: Absorption Cross Sections of *n*-Butyraldehyde and *i*-Butyraldehyde as a Function of Wavelength

λ (nm)	σ (*n*-butyraldehyde) (10^{-20} cm^2 molecule^{-1})	σ (*i*-butyraldehyde) (10^{-20} cm^2 molecule^{-1})
280	4.96 ± 0.06[a]	4.93 ± 0.13
285	5.85 ± 0.11	5.57 ± 0.03
290	5.88 ± 0.06	5.58 ± 0.08
295	6.14 ± 0.04	5.76 ± 0.01
300	5.82 ± 0.11	5.75 ± 0.20
305	5.68 ± 0.08	5.43 ± 0.14
310	4.17 ± 0.02	4.70 ± 0.14
315	3.38 ± 0.07	4.08 ± 0.13
320	2.28 ± 0.14	3.15 ± 0.27
325	1.86 ± 0.13	2.15 ± 0.10
330	1.11 ± 0.15	1.41 ± 0.21

[a] Uncertainty (1σ) represents experimental scatter.

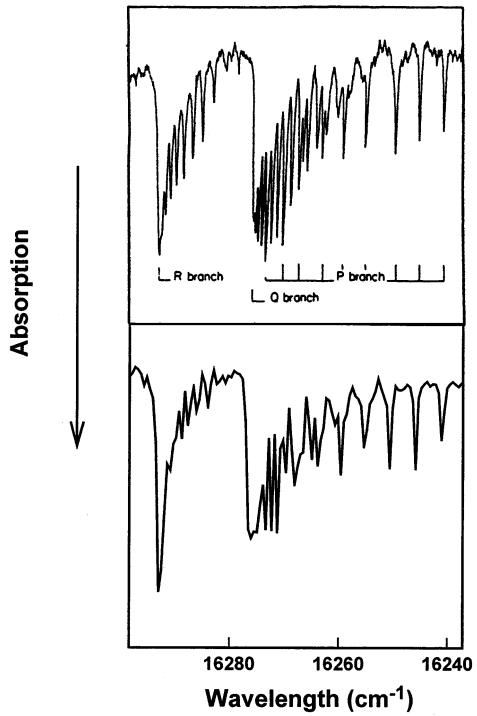

Figure 2. Upper panel: intracavity laser absorption spectrum of the (000) → (090) vibronic transition of HCO following photolysis of 0.1 Torr CH_3CHO/10 Torr Ar at 266 nm (adapted from ref 22). Lower panel: low-resolution cavity ring-down absorption spectrum of the product from 290-nm photolysis of 5.8 Torr of *i*-C_3H_7CHO.

butyraldehyde and *i*-butyraldehyde pressure in the cell and by applying Beer's law to the data. Error bars quoted (1σ) are the estimated precision of cross-section determinations, which include the standard deviation for each measurement (~0.5%) plus the standard deviation about the mean of at least four repeated experimental runs. Besides random errors, systematic errors also contribute to the uncertainty in cross-section values. The major sources of systematic errors are those involving pressure (0.1%) and path-length (0.2%) determinations and those resulting from the presence of impurities (<0.5%) in *n*-butyraldehyde and *i*-butyraldehyde. Adding relative (see Table 1) and systematic errors, the overall uncertainty for *n*-butyraldehyde and *i*-butyraldehyde cross-section measurements is about 5−10% for all wavelengths except 330 nm, where the overall measurement uncertainty is on the order of 15%. For comparison, cross-section results reported by Martinez and co-workers[16] (*n*-butyraldehyde and *i*-butyraldehyde) and by Tadic and co-workers[14] (*n*-butyraldehyde) are included in Figure 1. Our cross-section values for *n*-butyraldehyde agree to within 10% with those obtained previously in the 280−325-nm region and to within 25% at 330 nm.[16] Our cross-section data for *i*-butyraldehyde agree to within 10% with those obtained by Martinez and co-workers[16] in the 280−310-nm region and to within 15% at 315 nm, 25% at 320 and 325 nm, and 35% at 330 nm.

Time-Resolved Studies of the Photolysis of *n*-Butyraldehyde and *i*-Butyraldehyde in the 280−330-nm Region. Figure 2 shows a cavity ring-down absorption spectrum of the product after 290-nm photolysis of *i*-butyraldehyde. Also shown is a previously reported absorption spectrum of HCO in the same wavelength region.[22] A comparison of these two spectra indicates that the HCO radical is a photolysis product of *i*-butyraldehyde. A similar product absorption spectrum was also obtained from the photolysis of *n*-butyraldehyde. The cavity ring-down spectrometer was tuned to the HCO X^2A'' (0,0,0) → A^2A' (0,9,0) R bandhead at 613.8 nm, and the HCO concentration was followed as a function of time. Shown in Figure 3 is a temporal profile of HCO from 290-nm photolysis of 3 Torr *i*-butyraldehyde along with a fit of the HCO decay profile using the following kinetic scheme:

$$HCO + HCO \rightarrow H_2CO + CO \quad (5)$$

$$HCO + i\text{-}C_3H_7 \rightarrow \text{products} \quad (6)$$

$$i\text{-}C_3H_7 + i\text{-}C_3H_7 \rightarrow C_6H_{14} \quad (7a)$$

$$\rightarrow C_3H_6 + C_3H_8 \quad (7b)$$

$$HCO + i\text{-}C_3H_7CHO \rightarrow \text{products} \quad (8)$$

This modeling scheme assumes that the HCO + *i*-C_3H_7 channel is the only important radical-formation channel from the photolysis of *i*-butyraldehyde at 290 nm. (As described in a later section, the HCO yield from the photodissociation of *i*-butyraldehyde at 290 nm is 0.71, whereas the balance of the yield is attributed to the C_3H_8 + CO channel.) Also included in Figure 3 is a plot of the experimental ring-down time constant as a function of time. As can be seen from this Figure, HCO concentration decays to its $^1/_e$ value in about 145 μs, while the ring-down time constant varies from ~19 to ~25 μs in this interval. Time-resolved HCO decay profiles from the photodissociation of 3, 6, and 9 Torr *i*-butyraldehyde were compared with the calculated values by the ACUCHEM simulation program.[23] The following input parameters were used: rate constants for the HCO + HCO, HCO + *i*-C_3H_7, *i*-C_3H_7 + *i*-C_3H_7, and HCO + *i*-C_3H_7CHO reactions ($k_{HCO + HCO}$, $k_{HCO + i-C_3H_7}$, $k_{i-C_3H_7 + i-C_3H_7}$, and $k_{HCO + i-C_3H_7CHO}$) and the initial HCO concentration ($[HCO]_0$). Initial values of $k_{HCO + HCO}$, $k_{HCO + i-C_3H_7}$, and $k_{HCO + i-C_3H_7CHO}$ were input , and the simulated HCO profiles were compared with the experimental results. A value for $k_{i-C_3H_7 + i-C_3H_7}$ of 2.11×10^{-11} cm^3 molecule^{-1} s^{-1} was taken from the literature.[24] Values of $k_{HCO + HCO}$, $k_{HCO + i-C_3H_7}$, and $k_{HCO + i-C_3H_7CHO}$ were adjusted until optimum fits of experimental profiles were accomplished. Coefficients $k_{HCO + HCO}$, $k_{HCO + i-C_3H_7}$, and $k_{HCO+i-C_3H_7CHO}$ thus extracted are $(5.8 \pm 0.8) \times 10^{-11}$, $(4.4 \pm 0.6) \times 10^{-11}$, and $(1.7 \pm 0.3) \times 10^{-14}$ cm^3 molecule^{-1} s^{-1}, respectively, where the uncertainty (1σ) represents experimental scatter only. The HCO decay profiles at all three *i*-butyraldehyde pressures are well fitted by the extracted $k_{HCO + HCO}$, $k_{HCO + i-C_3H_7}$, and $k_{HCO + i-C_3H_7CHO}$ rate constants. The accuracy of $k_{HCO + HCO}$ and $k_{HCO + i-C_3H_7}$ measurements is affected by the accuracy in the determination

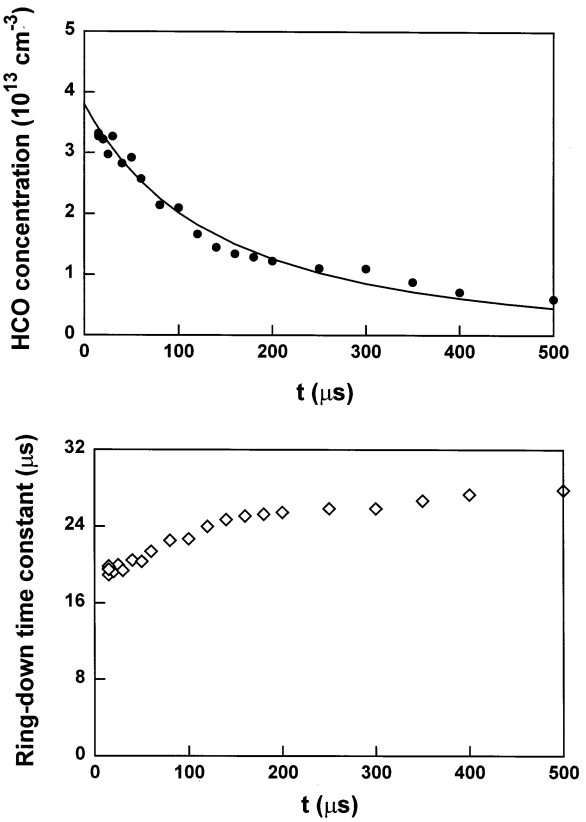

Figure 3. Upper panel: time profile of the HCO radical from the photolysis of 3 Torr of *i*-butyraldehyde at 290 nm: (●) experimental results; (—) calculated profile using the ACUCHEM simulation program. Lower panel: ring-down time constant as a function of time.

of the HCO absorption cross section (σ_{HCO}) and initial concentration and by the time resolution of the cavity ring-down spectroscopy (~19−29 μs near 613 nm). The σ_{HCO} value used in the calculation is $\sim 1.7 \times 10^{-18}$ cm^2/molecule. The initial HCO concentration was in the range of 3.7×10^{13} to 7.5×10^{13} cm^3 when the *i*-butyraldehyde pressure was varied between 3 and 9 Torr. The overall uncertainty in the extracted values of $k_{HCO + HCO}$ and $k_{HCO + i\text{-}C_3H_7}$ is about 50%. The extracted $k_{HCO + HCO}$ and $k_{HCO + i\text{-}C_3H_7}$ values agree well with the recommended rate constant[25] for the HCO + HCO reaction ($k = 2.5 \times 10^{-11}$ to 10.0×10^{-11} cm^3 molecule^{-1} s^{-1} at 300 K) and with the previously reported rate constant[26] for the HCO + *i*-C_3H_7 reaction ($(5.9 \pm 1.2) \times 10^{-11}$ cm^3 molecule^{-1} s^{-1}). The value of $k_{HCO + i\text{-}C_3H_7CHO}$ mainly influences the HCO decay profile when its time scale is on the order of hundreds of μs. Because the HCO decay profiles were measured at several *i*-butyraldehyde pressures under the condition that $[HCO]_0 \ll [i\text{-}C_3H_7CHO]_0$, the overall uncertainty in the $k_{HCO + i\text{-}C_3H_7CHO}$ value is ~20%. We have not attempted to measure the HCO + HCO, HCO + *n*-C_3H_7, and HCO + *n*-C_3H_7CHO rate constants from the photolysis of *n*-butyraldehyde because of the weaker HCO signal.

HCO Quantum Yields from the Photolysis of *n*-Butyraldehyde and *i*-Butyraldehyde in the 280−330-nm Region. The HCO quantum yields from the photolysis of *n*-butyraldehyde and *i*-butyraldehyde were determined from the ratio of the HCO concentration produced in the photolysis/probe laser overlapping region to the absorbed photon density in the same region. The overlapping region could be viewed as a rectangular solid with the center overlapped with that of the cell, with the width and height defined by the dimensions of the photolysis beam and length defined by (beam width) × $\tan(15°)^{-1}$, where 15° is the angle (≤±0.5° uncertainty in angle measurement) between the photolysis and the probe beams. The photolysis beam widths varied between 1.3 and 3.5 mm, depending on the identity of the laser dyes used, whereas the uncertainty in the beam width measurement is ~15%. Thus, the length of the photolysis/probe laser overlapping region is between 5.0 ± 0.8 and 13.5 ± 2.0 mm. The photolysis beam is absorbed by *n*-butyraldehyde or *i*-butyraldehyde over the entire level arm through which it travels. The absorbed photolysis photon density in the pump/probe laser overlapping region can be derived from the difference in the transmitted photolysis beam energy entering (E_{in}) and leaving (E_{out}) that region, the individual photon energy (hc/λ) at the photolysis wavelength (λ), and the volume (v) of the overlapping region by using the following equations:

$$\text{absorbed photon density} = \frac{E_{in} - E_{out}}{h\frac{c}{\lambda}v}$$

$$v = \text{beam width} \times \text{beam height} \times \text{length of the overlapping region}$$

The photolysis beam energy entering or leaving the pump/probe laser overlapping region can be calculated from the incident photolysis beam energy in the cell (E_0), the aldehyde absorption cross section (σ) and its density (n) in the cell, and the absorbing path length by using Beer's law:

$$E_{in} = E_0 \exp(-\sigma n l_1)$$

$$E_{out} = E_0 \exp(-\sigma n l_2)$$

l_1 is the distance between the photolysis beam entrance and the beginning of the pump/probe laser overlapping region. l_2 is the distance between the photolysis beam entrance and the end of the pump/probe laser overlapping region. The incident photolysis beam energy was measured by a calibrated joulemeter in front of the cell. The incident beam energy inside the cell was corrected for transmission loss at the front cell window (~8% correction) and for reflection of the photolysis beam from the rear cell window (4−9% correction). The HCO concentration after the photolysis was acquired by measuring its absorption at 613.80 nm at a photolysis and probe laser delay of 15 μs. To convert HCO absorption into absolute concentration, we determined the absorption cross section of HCO at the probe laser wavelength relative either to the formaldehyde photolysis reaction $H_2CO + h\nu \rightarrow HCO + H$, for which the HCO quantum yield is known,[25] or to the $Cl + H_2CO \rightarrow HCl + HCO$ reaction. In the 280−300-nm region, formaldehyde photolysis calibration was used. H_2CO was produced immediately prior to each calibration run in a glass bulb. The purity of the H_2CO was estimated by comparing its absorption cross sections with literature values.[27] The H_2CO absorption cross section was determined by measuring the transmitted photolysis photon fluence as a function of H_2CO pressure in the cell and by applying Beer's law to the data obtained. Our H_2CO cross sections (tabulated in Table 2) agree with those obtained by Meller and Moortgat[27] to within 10% at 280 and 295 nm, 15% at 300 nm, 20% at 290 nm, and 35% at 285 nm. Because the HCO absorption was measured 15 μs after the photolysis of H_2CO, the following sequence of reactions has been used to calculate the HCO concentration at $t = 15$ μs (the HCO concentration at $t = 0$ was calculated from the absorbed photon density in the photolysis/probe laser overlapping region and from

TABLE 2: Absorption Cross Sections of Formaldehyde and Chlorine

λ (nm)	σ_{H_2CO} (10^{-20} cm^2 molecule^{-1})	σ_{Cl_2} (10^{-20} cm^2 molecule^{-1})
280	2.10 ± 0.18[a]	
285	2.81 ± 0.10	
290	0.96 ± 0.12	
295	3.81 ± 0.37	
300	1.13 ± 0.07	11.4 ± 0.7
305		16.0 ± 0.1
310		17.0 ± 0.1
315		20.7 ± 1.0
320		23.0 ± 2.3
325		25.8 ± 0.6
330		25.4 ± 0.4

[a] Uncertainty (1σ) represents experimental scatter.

the literature[25] HCO yields from the H_2CO photolysis):

$$HCO + HCO \rightarrow H_2CO + CO \quad (5)$$

$$H + HCO \rightarrow H_2 + CO \quad (9)$$

$$H + H_2CO \rightarrow H_2 + HCO \quad (10)$$

The value of $k_{HCO + HCO} = 5.8 \times 10^{-11}$ cm^3 molecule^{-1} s^{-1} determined from this work was used in the fitting. Literature values of $k_{H + HCO} = 1.5 \times 10^{-10}$ cm^3 molecule^{-1} s^{-1} and $k_{H + H_2CO} = 3.8 \times 10^{-14}$ cm^3 molecule^{-1} s^{-1} were also used in the simulation.[28] In the 300−330-nm region, the absolute HCO concentration was calibrated relative to the Cl + H_2CO reaction. The Cl + H_2CO calibration was conducted by first introducing only H_2CO into the cell and determining the HCO radical absorption from the formaldehyde photolysis. Initial concentrations of HCO radicals ($[HCO]_0$) and hydrogen atoms ($[H]_0$) generated from the photolysis of formaldehyde were calculated. A mixture of chlorine (Cl_2) and H_2CO (an equal amount of H_2-CO, as in the formaldehyde photolysis) was subsequently introduced into the cell, and the HCO absorption 15 μs after the photolysis of a Cl_2/H_2CO mixture was measured. Values of the ratio of HCO absorption due to the photolysis of H_2CO to the absorption due to the photolysis of a Cl_2/H_2CO mixture were approximately 9−15, 9−46, 17−43, 26−52, 5−16, 4−10, and 3−16% at 300, 305, 310, 315, 320, 325, and 330 nm, respectively. Chlorine and formaldehyde were introduced into the cell at a pressure ratio of $P_{Cl_2}/P_{H_2CO} = 1{:}5$ ($P_{total} = 0.6$ and 1.2 Torr) to ensure that Cl atoms produced from the photolysis of Cl_2 reacted only with H_2CO. Absorption cross sections of Cl_2 were determined in the 300−330-nm region and are listed in Table 2. They agree with literature values[29] to within 10% at all wavelengths. The following sequence of reactions can occur 15 μs after the photolysis of a Cl_2/H_2CO mixture:

$$Cl + H_2CO \rightarrow HCl + HCO \quad (11)$$

$$Cl_2 + HCO \rightarrow HClCO + Cl^{\ddagger} \quad (12)$$

$$Cl^{\ddagger} + H_2CO \rightarrow HCl^{\ddagger} + HCO \quad (13)$$

$$H + Cl_2 \rightarrow HCl + Cl^* \quad (14)$$

$$Cl^* + H_2CO \rightarrow HCl^* + HCO \quad (15)$$

The chlorine atoms in eq 11 are generated from the photolysis of Cl_2, and those in eq 12 are a product of the reaction of Cl_2 with HCO. The chlorine atoms in eq 14 are a product of the reaction of Cl_2 with H atoms generated from formaldehyde photolysis. Reactions 13 and 15 represent the generation of HCO through reactions of secondary Cl atoms with H_2CO. The following parameters have been used in the ACCUCHEM program to calculate the HCO concentration 15 μs after the photolysis of a Cl_2/H_2CO mixture: the initial concentration of chlorine atoms ($[Cl]_0$) from the photolysis of Cl_2, the initial concentrations of formaldehyde ($[H_2CO]_0$) and chlorine ($[Cl_2]_0$), the initial concentrations of HCO radicals ($[HCO]_0$) and hydrogen atoms ($[H]_0$) from the formaldehyde photolysis, and the literature rate constants (in units of cm^3 molecule^{-1} s^{-1}) for the Cl + H_2CO (7.3×10^{-11}), HCO + Cl_2 (7.6×10^{-12}), and H + Cl_2 (2.0×10^{-11}) reactions.[25,30,31] The HCO absorption cross section (σ_{HCO}) was derived using the equation

$$A_{t=15\,\mu s} = \sigma_{HCO} \times [HCO]_{t=15\,\mu s} \times 2 \times l$$

where $A_{t=15\,\mu s}$ and $[HCO]_{t=15\,\mu s}$ are the round-trip HCO absorption and HCO concentration, respectively, 15 μs after the photolysis of a Cl_2/H_2CO mixture. l is the absorbing path length and is equal to (photolysis beam width)/sin 15°. To estimate the effect of sequential reactions, such as reactions 12 and 13 or reactions 14 and 15, toward HCO concentration 15 μs after the photolysis of a Cl_2/H_2CO mixture, we also ran simulations without including these processes.

Sequential reactions 12 and 13 decrease the HCO concentration by ∼2% under the experimental conditions used and have been corrected. Regeneration of HCO through reactions 14 and 15 increases the HCO concentration by 3−10% at 300 nm and in the 320−330-nm region. This correction of the HCO regeneration is 6−23% at 305 nm, 12−25% at 310 nm, and 14−27% at 315 nm. At 300 nm, both formaldehyde photolysis and the Cl + H_2CO reaction were used to calibrate the absolute HCO concentration. In these calibrations, the optical depth of formaldehyde was within a factor of 2 of that of Cl_2. The HCO absorption cross section obtained by these two methods agrees to within 10%. The value of the HCO cross section ranges from 1.6×10^{-18} to 2.0×10^{-18} cm^2 at 613.8 nm, with a measurement uncertainty of ∼20%.

The dependence of the HCO quantum yields on *n*-butyraldehyde and *i*-butyraldehyde pressures was examined by determinations of the HCO quantum yields from the photolysis of 1, 2, 4, 6, 8, and 10 Torr of *n*-butyraldehyde and *i*-butyraldehyde. Shown in Figure 4 are plots of the HCO quantum yields (φ_{HCO}) as a function of *i*-butyraldehyde pressure at photolysis wavelengths of 285 and 325 nm. φ_{HCO} decreases with increasing *i*-butyraldehyde pressure possibly because of the quenching of the excited *i*-butyraldehyde by the ground-state aldehyde molecules and the increasing HCO + HCO, HCO + *i*-C_3H_7, and HCO + *i*-C_3H_7CHO reactions at higher aldehyde pressures. To separate the contribution of HCO radical reactions from that of the quenching process, we include in Figure 4 both the uncorrected HCO yields and the yields that have been corrected for HCO radical reactions at 15 μs. As can be seen from this Figure, there was no *i*-butyraldehyde pressure quenching effect when the photolysis study was conducted at 285 nm. The corrected HCO quantum yields still decrease with increasing aldehyde pressure at 325 nm, suggesting an *i*-butyraldehyde pressure quenching effect at longer photolysis wavelengths. Because 325 nm is close to the photodissociation threshold of *i*-butyraldehyde, increasing *i*-butyraldehyde pressure quenches the excited molecule to below its dissociation limit. The corrected reciprocal HCO yields were plotted against *i*-butyral-

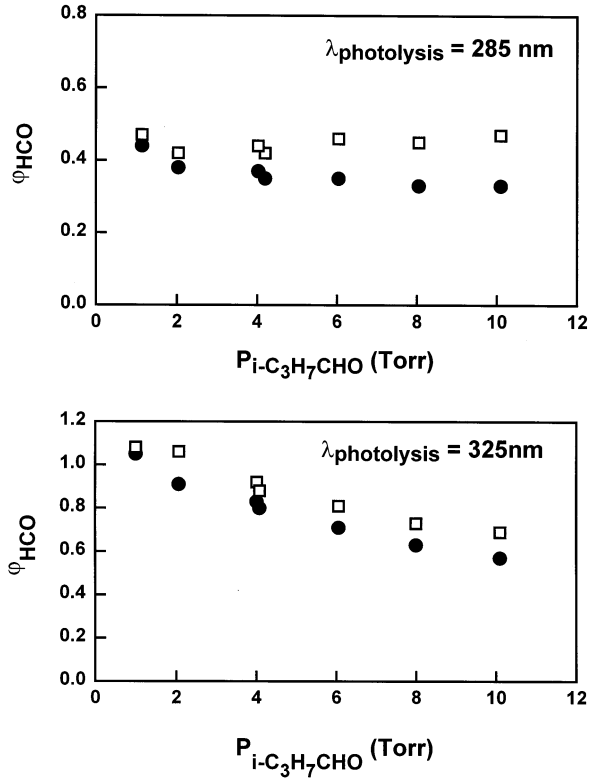

Figure 4. HCO quantum yields as a function of i-C_3H_7CHO pressure at the 285-nm (upper panel) and 325-nm (lower panel) photolysis wavelengths: (●) uncorrected yields; (□) yields that have been corrected for the HCO + HCO, HCO + i-C_3H_7, and HCO + i-C_3H_7-CHO reactions at 15 μs.

dehyde concentration ([i-C_3H_7CHO]) according to the Stern−Volmer equation:

$$1/\varphi_{HCO} = 1/\varphi^0_{HCO} + (k^Q_{i-C_3H_7CHO}/k^D_{i-C_3H_7CHO})[i\text{-}C_3H_7CHO]$$

φ^0_{HCO} is the HCO quantum yield extrapolated to zero i-butyraldehyde pressure, and $k^Q_{i-C_3H_7CHO}/k^D_{i-C_3H_7CHO}$ is the ratio of quenching to the unimolecular decay rate constant of excited i-butyraldehyde. For those photodissociation wavelengths at which the corrected HCO quantum yields are independent of i-butyraldehyde pressure, $k^Q_{i-C_3H_7CHO}/k^D_{i-C_3H_7CHO}$ is set equal to zero. Shown in Figure 5 is a linear plot of $1/\varphi_{HCO}$ versus [i-C_3H_7CHO] that was obtained from the 325-nm photolysis of i-C_3H_7CHO. Values of φ^0_{HCO} and k^Q/k^D for n-butyraldehyde and i-butyraldehyde as a function of the photolysis wavelength are tabulated in Table 3 and plotted in Figure 6 (φ^0_{HCO} only). $k^D_{n-C_3H_7CHO}$ has been reported to be approximately 2.2×10^8 s^{-1} for excited n-butyraldehyde (S_1 state, $E_{vib} \approx 0$), which corresponds to an excited-state decay lifetime of about 4.5 ns.[32] $k^Q_{n-C_3H_7CHO}$ is on the order of 1.9×10^{-10} to 5.7×10^{-10} cm^3 $molecule^{-1}$ s^{-1}. Assuming a $k^D_{i-C_3H_7CHO}$ value of 2.2×10^8 s^{-1}, $k^Q_{i-C_3H_7CHO}$ is on the order of 1.9×10^{-10} to 4.4×10^{-10} cm^3 $molecule^{-1}$ s^{-1}. The magnitudes of $k^Q_{n-C_3H_7CHO}$ and $k^Q_{i-C_3H_7CHO}$ are reasonable because an electronic-to-vibrational energy transfer (E → V) can occur on a single-collision time scale. As seen from Figure 6, the zero pressure HCO quantum yields from n-butyraldehyde and i-butyraldehyde photolysis display significant wavelength dependencies and decrease at both the longer- and the shorter-wavelength ends. The decrease in HCO quantum yields with decreasing wavelength at the shorter-wavelength end can possibly be attributed to the opening up of an additional photodissociation pathway, such as the formation of C_3H_8 + CO, at higher photon energy. The reduced HCO quantum yields at the longer-wavelength tail may be the result of dissociation at near-threshold wavelengths. The peak HCO quantum yield from n-butyraldehyde photolysis is 0.84 ± 0.04, whereas that from i-butyraldehyde photolysis is 1.10 ± 0.10. The difference in the peak HCO quantum yields from n- and i-butyraldehyde photolysis is attributed to the opening up of the Norrish II channel for n-butyraldehyde. Error bars were calculated using cumulative error analysis of the standard deviations of at least two $1/\varphi_{HCO}$ versus [C_3H_7CHO] plots. Systematic errors include uncertainties in the determination of the following parameters: HCO absorption cross section (∼20%), n-butyraldehyde or i-butyraldehyde concentration and cross section (∼10%), pulse energy (∼5%), angle between the photolysis and the probe lasers (3%), and the dye laser width. Because the HCO quantum yields from the photolysis of n- and i-butyraldehyde were determined relative to those obtained from H_2CO photolysis or from the Cl + H_2CO reaction, the uncertainty in the dye laser width measurement should not directly affect the relative HCO quantum yields, although it will affect the correction of the HCO radical reactions. As a result, the uncertainty in the dye laser width will indirectly affect the yield data. Adding the relative (∼10%) and systematic errors, the overall uncertainty in the determination of φ^0_{HCO} is about 50% in the wavelength range that was studied.

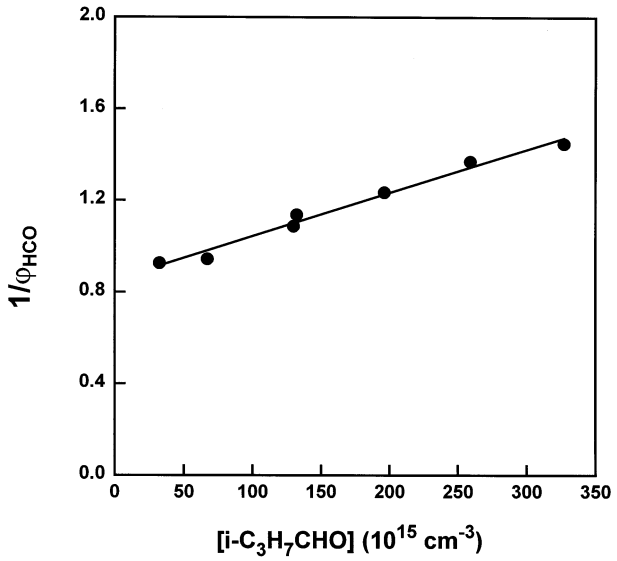

Figure 5. Stern−Volmer plot of the reciprocal HCO quantum yields as a function of i-C_3H_7CHO concentration at the 325-nm photolysis wavelength: (●) experimental data; (—) fit of the data to the Stern−Volmer expression.

We examined the dependence of the HCO quantum yields on the total pressure by maintaining a constant n- or i-butyraldehyde pressure and varying the nitrogen buffer-gas pressure. The HCO quantum yields were found to be independent of the total pressure to within the experimental error limit when the total pressure was varied from 8 to 400 Torr in the 280−330-nm region. In the presence of excess nitrogen, a relatively inefficient electronic-to-rotational/translational energy transfer (E → R/T) and a vibrational-to-rotational/translational energy transfer (V → R/T) between the vibronically excited n- or i-butyraldehyde and nitrogen could occur. In the case of the photolysis of several Torr of n- or i-butyraldehyde, an efficient electronic-to-vibrational energy transfer (E → V) and a resonant vibrational-to-vibrational energy transfer (V → V) between the excited- and the ground-state aldehyde might occur. Therefore, there would not necessarily be a contradiction between the

TABLE 3: Values of φ^0_{HCO} and k^Q/k^D from the Photolysis of *n*-Butyraldehyde and *i*-Butyraldehyde

λ (nm)	φ^0_{HCO} (*n*-butyraldehyde)	k^Q/k^D (*n*-butyraldehyde) (10^{-18} cm^3/molecule)	φ^0_{HCO} (*i*-butyraldehyde)	k^Q/k^D (*i*-butyraldehyde) (10^{-18} cm^3/molecule)
280	0.22 ± 0.02[a]	0	0.31 ± 0.04	0
285	0.24 ± 0.02	0	0.50 ± 0.07	0
290	0.28 ± 0.04	0	0.71 ± 0.04	0
295	0.30 ± 0.04	0	0.91 ± 0.04	0
300	0.31 ± 0.04	0	1.00 ± 0.14	0
305	0.52 ± 0.05	0	0.92 ± 0.08	0
310	0.74 ± 0.08	0.87 ± 0.54	1.06 ± 0.07	0.86 ± 0.31
315	0.84 ± 0.04	1.2 ± 0.5	1.06 ± 0.13	1.2 ± 0.7
320	0.77 ± 0.08	2.0 ± 1.2	1.10 ± 0.10	1.4 ± 0.5
325	0.74 ± 0.06	2.1 ± 0.6	1.10 ± 0.10	1.9 ± 0.5
330	0.59 ± 0.10	2.6 ± 1.7	0.94 ± 0.06	2.0 ± 0.6

[a] Uncertainty (1σ) represents experimental scatter.

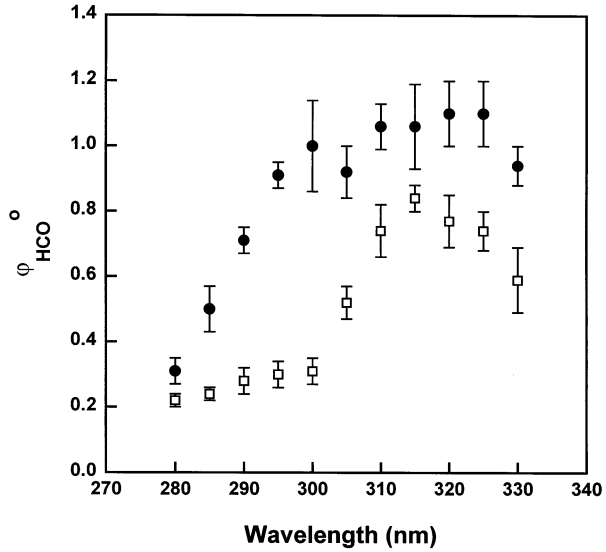

Figure 6. Zero-pressure HCO quantum yields as a function of photodissociation wavelength: (□) *n*-butyraldehyde; (●) *i*-butyraldehyde.

observation of pressure quenching by *n*-butyraldehyde and *i*-butyraldehyde at several Torr and the absence of pressure quenching by nitrogen at pressures up to 400 Torr. The-zero pressure HCO quantum yields were set equal to those obtained from the photolysis of *n*-butyraldehyde and *i*-butyraldehyde at 760 Torr of nitrogen.

Förgeteg and co-workers[13] investigated the photolysis of *n*-butyraldehyde at 313 nm by analyzing the yields of 20 end-products from the photodissociation process. The primary photolysis pathways were found to be n-$C_3H_7CHO + h\nu \rightarrow n$-$C_3H_7$ + HCO ($\varphi = 0.34$) and n-$C_3H_7CHO + h\nu \rightarrow C_2H_4 + CH_3CHO$ ($\varphi = 0.17$). The zero-pressure HCO yield (0.80) at 313 nm obtained from the present work is 2.4 times that obtained by Förgeteg and co-workers. Because the previous work is an indirect study conducted at an *n*-butyraldehyde pressure of 100 Torr, it is subject to more uncertainty. Tadic and co-workers[14] recently characterized the photooxidation of *n*-butyraldehyde in air by combining UV lamp photolysis with FTIR. Products observed include CO, ethene, vinyl alcohol, and acetaldehyde. The yield of the radical channel or Norrish II channel was derived from the ratio of the amount of CO or ethene formed to the amount of *n*-butyraldehyde consumed. The relative yield of the radical channel versus the Norrish II channel was 68%: 32%. The average total photolysis quantum yield from 275−380 nm was 0.48 in 100 Torr of air and 0.38 in 700 Torr of air. Both the HCO + C_3H_7 channel and the CO + C_3H_8 channel lead to the formation of CO when *n*-butyraldehyde is photolyzed in air. The relative contribution of the HCO + C_3H_7 channel versus that of the CO + C_3H_8 channel was not reported from the previous work. As a result, a direct comparison with our HCO yield is not possible. Our HCO yield that was averaged over the 280−330-nm range is 0.50. We did not observe any dependence of the HCO yield on nitrogen buffer gas pressure in the 8−400-Torr range.

TABLE 4: Values of φ_{HCO} from the Photolysis of *i*-Butyraldehyde

λ (nm)	φ_{HCO}[a]	λ (nm)	φ_{HCO}[b]
253.7	0.20	280	0.31 ± 0.04[c]
280.3	0.45	285	0.50 ± 0.07
302.2	0.55	290	0.71 ± 0.04
312.8	0.88	295	0.91 ± 0.04
326.1	0.88	300	1.00 ± 0.14
334.1	0.69	305	0.92 ± 0.08
		310	1.06 ± 0.07
		315	1.06 ± 0.13
		320	1.10 ± 0.10
		325	1.10 ± 0.10
		330	0.94 ± 0.06

[a] HCO quantum yields in 1 atm of air by Desai and co-workers.[15] [b] HCO quantum yields in 1 atm of nitrogen from this work. [c] Uncertainty (1σ) represents experimental scatter.

Desai and co-workers[15] studied the photolysis of *i*-butyraldehyde in oxygen at several incident wavelengths. The quantum yields for the i-$C_3H_7CHO + h\nu \rightarrow i$-$C_3H_7$ + HCO channel were deduced from the difference in the quantum yields of CO and C_3H_8. Their HCO yields in 1 atm of air were 0.20, 0.45, 0.55, 0.88, 0.88, and 0.69 at 253.7, 280.3, 302.2, 312.8, 326.1, and 334.1 nm, respectively. These data are listed in Table 4 and are compared with our data in Figure 7. As seen from the Figure, there is a good agreement between our HCO yields and those obtained by Desai and co-workers[15] at 312.8 and 326.1 nm. The HCO yields obtained previously were 29% higher than our value at 280.3 nm and 43% lower than our value at 302.2 nm. The HCO yield at 302.2 nm obtained by Desai and co-workers[15] seems to deviate from the curve defined by their other data points. The reason for this discord is unclear.

Comparison with the Photolysis of Other Aldehydes. The photodissociation of *n*-butyraldehyde is compared with the photodissociation of *n*-pentanal and *i*-pentanal.[11,12] Shown in Figure 8 are the HCO quantum yields as a function of wavelength from the photolysis of *n*-butyraldehyde, *n*-pentanal, and *i*-pentanal. The shape of the HCO yields versus wavelength curve is similar for all three aldehydes. However, the peak radical yields are very different. The peak radical yields from the photolysis of *n*-butyraldehyde, *n*-pentanal, and *i*-pentanal are 0.84 ± 0.04, 0.20 ± 0.06, and 0.40 ± 0.08, respectively.

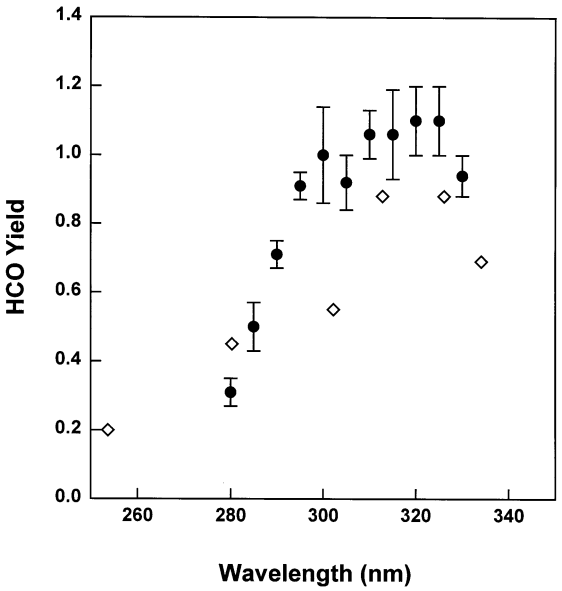

Figure 7. HCO quantum yields from the photolysis of *i*-butyraldehyde: (●) HCO yields in 1 atm of nitrogen from this work; (◊) HCO yields in 1 atm of air from Desai and co-workers.[15]

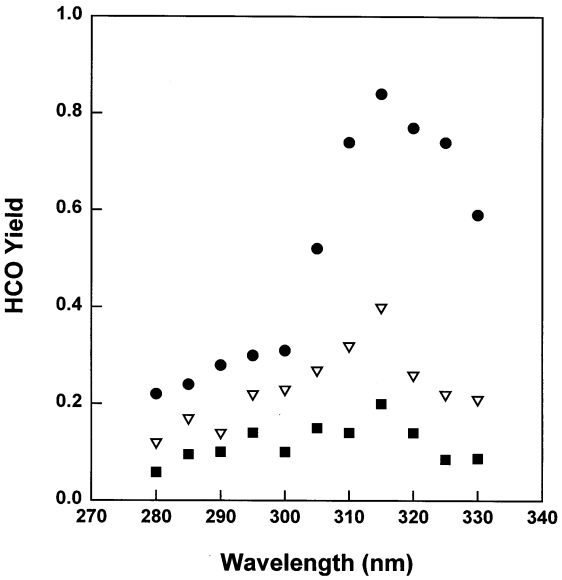

Figure 8. Wavelength dependence of the HCO quantum yields from the photolysis of *n*-butyraldehyde, *n*-pentanal, and *i*-pentanal: (●) *n*-butyraldehyde from this work; (■) *n*-pentanal;[11] (▽) *i*-pentanal.[12]

The difference in the peak radical yields can be attributed to the difference in the extent of the Norrish II channel from the photolysis of these three aldehydes. A comparison of the radical yields from the photolysis of *n*-butyraldehyde and *n*-pentanal seems to indicate that the yields of the Norrish II channel increase with carbon chain length.

Figure 9 shows radical yields as a function of wavelength from the photolysis of *i*-butyraldehyde, along with our earlier results from the photolysis of propionaldehyde[10] and t-pentanal.[12] The peak radical yields from the photolysis of all three aldehydes are approximately unity. However, the decay of radical yields with decreasing wavelength is faster for t-pentanal and *i*-butyraldehyde than for propionaldehyde. Radical products have been postulated to result from dissociation at the excited triplet surface.[32] The formation of alkane + CO has been correlated with dissociation at an excited singlet surface, and this channel opens up only at higher photon energies. The

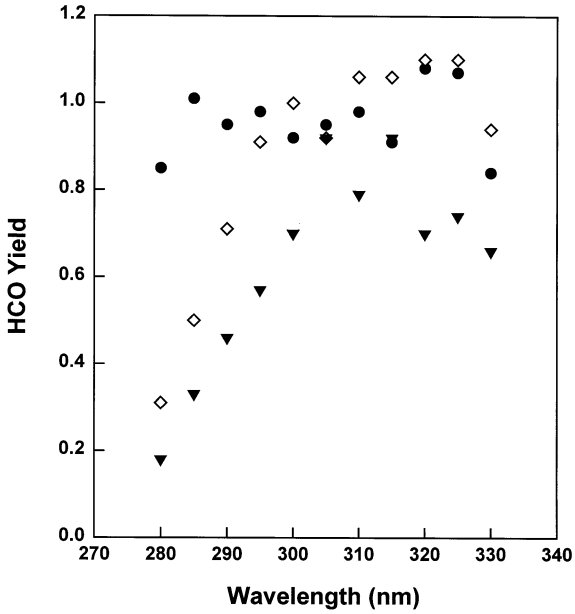

Figure 9. Wavelength dependence of the HCO quantum yields from the photolysis of propionaldehyde, *i*-butyraldehyde, and *t*-pentanal. (●) propionaldehyde;[10] (◊) *i*-butyraldehyde from this work; (▼) *t*-pentanal.[12]

difference in the falloff behavior at shorter photodissociation wavelengths may reflect difference in the excited states' singlet−triplet surface crossing of molecules.

End-Product Studies. *n*-Butyraldehyde and *i*-butyraldehyde were photolyzed in a closed cell at 290, 310, and 330 nm. The photolysis end-products were analyzed by a residual gas analyzer mass spectrometer connected to the cell. *n*-Butyraldehyde and *i*-butyraldehyde pressures of 4 Torr each were used in the experiments. The mass spectra peak intensity at $m/e = 28$ increased after the photolysis of *n*-butyraldehyde and *i*-butyraldehyde, which would correlate with photodissociation products such as HCO, C_2H_4, and CO. The product quantum yields at $m/e = 28$ result from the sum of the yields of radical-formation (HCO + C_3H_7), Norrish II (C_2H_4 + CH_3CHO), and molecular-elimination (C_3H_8 + CO, available at short wavelengths) channels. For *i*-butyraldehyde photolysis at 310 and 330 nm, only the radical-formation channel is available, and its yield is equal to $\varphi_{m/e=28}$. For *n*-butyraldehyde photolysis at 310 and 330 nm, both the radical-formation and the Norrish II channels are available, and the product yields at $m/e = 28$ result from the sum of the yields of these two channels. By subtraction of the yields of the radical-formation channel at 290, 310, and 330 nm, the yields of the Norrish II channel from *n*-butyraldehyde photolysis were estimated; they are 55, 52, and 56% at 290, 310, and 330 nm, respectively. The Norrish II yield at 290 nm may include some contribution from the C_3H_8 + CO channel because this channel opens up at shorter photolysis wavelengths.

To examine the effect of oxygen pressure on the yields of photolysis end-products, we conducted end-product studies by using oxygen at various pressures as the carrier gas, and then we determined its effect on the yield of $m/e = 28$ components (CO and C_2H_4 detection for *n*-butyraldehyde; CO detection for *i*-butyraldehyde) after photolysis of *n*-butyraldehyde and *i*-butyraldehyde. The experiment was not successful because of the large CO background resulting from ion−molecule reactions in the ionization region of the mass spectrometer into which an unphotolyzed butyraldehyde/O_2 mixture was introduced. We also attempted to monitor acetaldehyde yield ($m/e = 44$) from the photolysis of *n*-butyraldehyde as a function of oxygen pressure. Because the mass spectrum of *n*-butyraldehyde has a

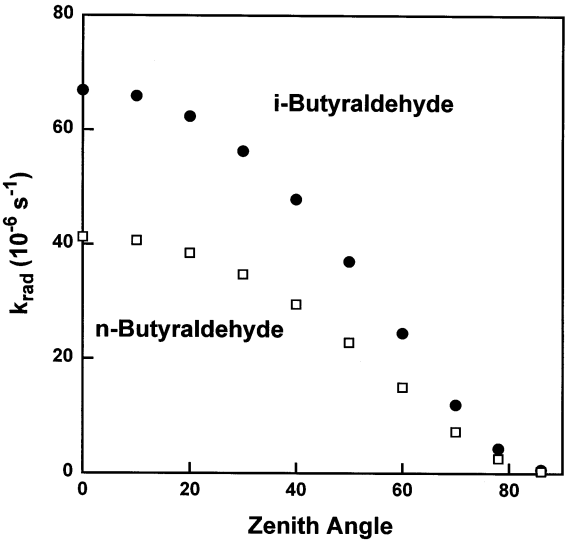

Figure 10. Atmospheric photodissociation rate constants for the formation of radicals as a function of zenith angle at 760 Torr of nitrogen: (□) *n*-butyraldehyde; (●) *i*-butyraldehyde.

strong fragment peak at mass 44, it was hard to separate by mass the acetaldehyde that is formed from the photolysis from the parent *n*-butyraldehyde. With GC−MS, it would be possible to separate the mass spectra of the parent molecule and its secondary product. However, we do not have this capability.

Photodissociation Rate Constants to Form HCO Radicals in the Atmosphere. The atmospheric photodissociation rate constants (k_{rad}) for HCO production (or production of HO_2 in the presence of air) from the photolysis of *n*-butyraldehyde and *i*-butyraldehyde were calculated from the actinic solar flux ($J(\lambda)$) reported by Demerjian and co-workers,[33] the absorption cross sections of *n*-butyraldehyde and *i*-butyraldehyde ($\sigma(\lambda)$), and the HCO radical yield at 760 Torr of nitrogen ($\varphi(\text{rad}, \lambda)$) using the relationship

$$k_{rad} = \Sigma\sigma(\lambda)\ \varphi(\text{rad}, \lambda)\ J(\lambda)\Delta\lambda$$

Radical-formation rate constants from the photodissociation of *n*-butyraldehyde and *i*-butyraldehyde were computed as a function of the zenith angle under cloudless conditions at sea level and for best-estimate albedo (5% in the 290−400 nm region[34]); the results are shown in Figure 10. Our estimated radical-formation rate constants for zenith angles in the 30−60° range are 3.5×10^{-5} to 1.5×10^{-5} s^{-1} for *n*-butyraldehyde and 5.6×10^{-5} to 2.4×10^{-5} s^{-1} for *i*-butyraldehyde. Desai and co-workers[15] reported radical-formation rate constants of 7.6×10^{-5} s^{-1} and 5.9×10^{-5} s^{-1} from the photolysis of *i*-butyraldehyde at zenith angles of 30° and 58.18°. Their radical-formation rate constants were calculated using old flux data,[35] which differ by a factor of 2 at certain wavelength intervals from the flux data reported in ref 33. Although the Norrish II process does not lead to the production of radicals, it can be a source of acetaldehyde in the atmosphere, and it affects the photolysis lifetime of *n*-butyraldehyde. By assuming a photolysis quantum yield of unity in the actinic UV region for *n*-butyraldehyde and *i*-butyraldehyde. The corresponding atmospheric photodissociation lifetimes of *n*-butyraldehyde and *i*-butyraldehyde are on the order of 4.9−13.7 h and 4.1−11.2 h for zenith angles from 0−60°. Literature rate constants[1,3,5,36−38] for OH radical reactions with *n*-butyraldehyde and *i*-butyraldehyde are on the order of 2.4×10^{-11} and 2.6×10^{-11} cm^3 $molecule^{-1}$ s^{-1}, which correspond to OH radical reaction lifetimes of 11.6 h and 10.7 h for a globally averaged OH radical concentration of 10^6 molecules cm^{-3}. Thus, both photolysis and OH radical reactions are important in removing *n*-butyraldehyde and *i*-butyraldehyde from the atmosphere.

Acknowledgment. We thank Dr. Liang T. Chu and Mr. Michael Force for helpful discussions about mass spectrometry. We are grateful for the support provided by the National Science Foundation under grant ATM-0000252.

References and Notes

(1) Semmes, D. H.; Ravishankara, A. R.; Gump-Perkins, C. A.; Wine, P. H. *Int. J. Chem. Kinet.* **1985**, *17*, 303.
(2) Dóbé, S.; Khachatryan, L. A.; Bérces, T. *Ber. Bunsen-Ges. Phys. Chem.* **1989**, *93*, 847.
(3) Kerr, J. A.; Sheppard, D. W. *Environ. Sci. Technol.* **1981**, *15*, 960.
(4) Tyndall, G. S.; Staffelbach, T. A.; Orlando, J. J.; Calvert, J. G. *Int. J. Chem. Kinet.* **1995**, *27*, 1009.
(5) Thévenet, R.; Mellouki, A.; LeBras, G. *Int. J. Chem. Kinet.* **2000**, *32*, 676.
(6) Moortgat, G. K.; Seiler, W.; Warneck, P. *J. Chem. Phys.* **1983**, *78*, 1185.
(7) Carmely, Y.; Horowitz, A. *Int. J. Chem. Kinet.* **1984**, *16*, 1585.
(8) Ho, P.; Bamford, D. J.; Buss, R. J.; Lee, Y. T.; Moore, C. B. *J. Chem. Phys.* **1982**, *76*, 3630.
(9) Horowitz, A.; Calvert, J. G. *J. Phys. Chem.* **1982**, *86*, 3105.
(10) Chen, Y.; Zhu, L. *J. Phys. Chem. A* **2001**, *105*, 9689.
(11) Cronin, T. J.; Zhu, L. *J. Phys. Chem. A* **1998**, *102*, 10274.
(12) Zhu, L.; Cronin, T.; Narang, A. *J. Phys. Chem. A* **1999**, *103*, 7248.
(13) Förgeteg, S.; Bérces, T.; Dóbé, S. *Int. J. Chem. Kinet.* **1979**, *11*, 219.
(14) Tadic, J.; Juranic, I.; Moortgat, G. K. *J. Photochem. Photobiol., A* **2001**, *143*, 169.
(15) Desai, J.; Heicklen, J.; Bahta, A.; Simonaitis, R. *J. Photochem.* **1986**, *34*, 137.
(16) Martinez, R. D.; Buitrago, A. A.; Howell, N. W.; Hearn, C. H.; Joens, J. A. *Atmos. Environ., Part A* **1992**, *26*, 785.
(17) Calvert, J. G.; Pitts, J. N., Jr. *Photochemistry*; Wiley: New York, 1966.
(18) O'Keefe, A.; Deacon, D. A. G. *Rev. Sci. Instrum.* **1988**, *59*, 2544.
(19) O'Keefe, A.; Scherer, J. J.; Cooksy, A. L.; Sheeks, R.; Heath, J.; Saykally, R. J. *Chem. Phys. Lett.* **1990**, *172*, 214.
(20) Zhu, L.; Johnston, G. *J. Phys. Chem. A* **1995**, *99*, 15114.
(21) Zhu, L.; Kellis, D.; Ding, C.-F. *Chem. Phys. Lett.* **1996**, *257*, 487.
(22) Stoeckel, F.; Schuh, M. D.; Goldstein, N.; Atkinson, G. H. *Chem. Phys.* **1985**, *95*, 135.
(23) Braun, W.; Herron, J. T. *ACUCHEM/ACUPLOT*; computer program for modeling complex reaction systems; National Bureau Of Standards: Gaithersburg, MD, 1986.
(24) Adachi, H.; Basco, N. *Int. J. Chem. Kinet.* **1981**, *13*, 367.
(25) Atkinson, R.; Baulch, D. L.; Cox, R. A.; Hampson, R. F., Jr.; Kerr, J. A.; Troe, J. *J. Phys. Chem. Ref. Data* **1992**, *21*, 1125.
(26) Baggott, J. E.; Frey, H. M.; Lightfoot, P. D.; Walsh, R. *J. Phys. Chem.* **1987**, *91*, 3386.
(27) Meller, R.; Moortgat, G. K. *J. Geophys. Res.* **2000**, *105*, 7089.
(28) Baulch, D. L.; Cobos, C. J.; Cox, R. A.; Esser, C.; Frank, P.; Just, Th.; Kerr, J. A.; Pilling, M. J.; Troe, J.; Walker, R. W.; Warnatz, J. *J. Phys. Chem. Ref. Data* **1992**, *21*, 411.
(29) Maric, D.; Burrows, J. P.; Meller, R.; Moortgat, G. K. *J. Photochem. Photobiol., A* **1993**, *70*, 205.
(30) Ninomiya, Y.; Goto, M.; Hashimoto, S.; Kagawa, Y.; Yoshizawa, K.; Kawasaki, M.; Wallington, T. J.; Hurley, M. D. *J. Phys. Chem. A* **2000**, *104*, 7556.
(31) Seeley, J. V.; Jayne, J. T.; Molina, M. J. *Int. J. Chem. Kinet.* **1993**, *25*, 571.
(32) Lee, E. K. C.; Lewis, R. S. *Adv. Photochem.* **1980**, *12*, 1.
(33) Demerjian, K. L.; Schere, K. L.; Peterson, J. T. *Adv. Environ. Sci. Technol.* **1980**, *10*, 369.
(34) Coulson, K. L.; Reynolds, D. W. *J. Appl. Meteorol.* **1971**, *10*, 1285.
(35) Wuebbles, D. Personal communication, 1981 (see ref 14).
(36) D'Anna, B.; Andresen, Ø.; Gefen, Z.; Nielsen, C. J. *Phys. Chem. Chem. Phys.* **2001**, *3*, 3057.
(37) Papagni, C.; Arey, J.; Atkinson, R. *Int. J. Chem. Kinet.* **2000**, *32*, 79.
(38) Stemmler, K.; Mengon, W.; Kerr, J. *J. Chem. Soc., Faraday Trans.* **1997**, *93*, 2865.